Impacts of User Mobility on URLLC System Performance Metrics over Time-Varying Channels

Yang Ou[1,2], Jie Huang[1,2*], Shuaifei Chen[2,1], Songjiang Yang[2,1], and Cheng-Xiang Wang[1,2*]
[1]National Mobile Communications Research Laboratory, School of Information Science and Engineering, Southeast University, Nanjing 210096, China.
[2]Purple Mountain Laboratories, Nanjing 211111, China.
*Corresponding Authors
Email: {yang_ou, j_huang, shuaifeichen}@seu.edu.cn, Yangsongjiang@pmlabs.com.cn, chxwang@seu.edu.cn

***Abstract*—In this paper, we study the impacts of user mobility on the average bit error probability (ABEP) and average achievable data rate (ADR) of ultra-reliable and low-latency communication (uRLLC) systems. Specifically, based on the time autocorrelation function (ACF) of the sixth generation pervasive channel model (6GPCM), we derive the expression of the pairwise error probability (PEP) of uRLLC systems adopting the M-ary phase shift keying (MPSK) modulation. In addition, we propose a new framework for the calculation of the average ADR considering the channel estimation period and cyclic prefix (CP) length. Moreover, the calculation methods of maximal data transmission period and transmission latency are given. Numerical results show that the increasing user mobility degrades the ABEP and average ADR. Impacts of user mobility on the ABEP surpass its influences on the average ADR. Furthermore, the tightness of analytical results is validated by Monte Carlo simulations. The performance analysis will guide the flexible designs of transmission blocklength under different reliability constraints.**

***Index Terms*—Performance analysis, uRLLC system, channel time ACF, user mobility, PEP.**

I. Introduction

The uRLLC is one of the most significant application scenarios for the fifth generation (5G) wireless communication, which will be further enhanced in the upcoming sixth generation (6G) wireless communication [1]. The reliability and latency are considered as two fundamental performance metrics of uRLLC systems [2]. The ABEP can be employed to characterize the reliability of uRLLC systems [3]. In addition, the effectiveness serving as another important performance metric of uRLLC systems is represented by the average ADR, which cannot be ignored [4].

In order to support uRLLC, various potential technologies were investigated. The short block transmission has been considered as the most promising technology to enable uRLLC among these technologies [5]. The expression of ADR was given in the short blocklength regime over the additive white Gaussian noise (AWGN) channel [6]. Expressions of multiple-antenna AWGN channel dispersion characteristics and capacity of short block transmission system were derived in [7]. Multiple traditional fading models were unified by the $\kappa-\mu$ fading channel model with short blocklength in [8].

The short block transmission assumes that the channel is quasi-static during the entire short block transmission period. However, the actual channel is time-varying, resulting in the imperfect channel state information (CSI) from the channel estimation. Therefore, employing the imperfect CSI will lead to the BEP deteriorating. Specifically, a model of channel estimation error based on channel time ACF was proposed [9]. Furthermore, the relationship between the ABEP and channel time ACF was studied in [10].

Meanwhile, the geometry based stochastic model (GBSM) is a wireless channel model describing geometrical relationships between transmitter (Tx), receiver (Rx), and scatterers. Compared to traditional fading channel models, it can characterize statistical properties of actual channels more accurately [11]. As one of GBSMs, the 6GPCM for all frequency bands and all scenarios was presented in [12]. Furthermore, its space-time-frequency (STF) statistical properties were completely studied in [13]. Specifically, relationships between channel statistical properties and environmental parameters were clearly shown. Impacts of spatial correlation functions on the ABEP in the vehicle-to-vehicle (V2V) scenario were revealed in [14]. However, the mobility mainly affects the channel time ACFs instead of spatial correlation functions.

To the best of the authors' knowledge, the performance analysis framework for user mobility, channel time ACF, and system performance metrics is still missing in the literature. The main contributions and novelties of our work are summarized as follows.

- The expression of the PEP of uRLLC systems utilizing the MPSK modulation is derived in mobility scenarios. The tightness of analytical results is validated by Monte Carlo simulations.
- The framework for calculation of the average ADR considering the channel estimation period and CP length is proposed. Meanwhile, the maximal transmission period under the reliability constraint is given.
- Performance metrics with different speeds of the moving user, i.e., the ABEP, maximal transmission periods, ratios of average ADR to average capacity, and transmission latency, are simulated and analyzed.

The remainder of this paper is organized as follows. Sec-

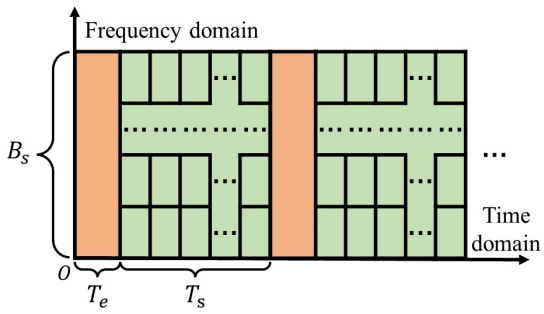

Fig. 1. Illustration of transmission periods.

tion II introduces the uRLLC system model considering the time-varying channel model. In Section III, uRLLC system performance metrics are introduced and derived. Results and analysis are presented in Section IV. Finally, conclusions are drawn in Section V.

II. System Model & Channel Model

A. URLLC System Model

We consider a multiple-input multiple-output (MIMO) orthogonal frequency-division multiplexing (OFDM) link from the base station (BS) to a moving vehicle user in the urban microcell (UMi) scenario. The BS is equipped with N_t antennas, while the vehicle has N_r antennas. In order to meet the requirements of uRLLC, the BS transmits signals through short blocks. For simplicity, we assume all signals are transmitted with the same blocklength. The blocklength N_b of the transmission signal can be defined as

$$N_b = B_s \cdot T_s \tag{1}$$

where B_s means the signal bandwidth and T_s denotes the signal duration.

Furthermore, $B_s = n_f \cdot \Delta f$ and $T_s = n_{\text{slot}} \cdot T_{\text{slot}}$, where Δf denotes the subcarrier spacing, T_{slot} means the slot duration, n_f and n_{slot} are numbers of subcarriers and slots of each signal, respectively. Specifically, $T_{\text{slot}} = n_{\text{sym}} \cdot (T_{\text{data}} + T_{\text{cp}})$, where n_{sym} means the number of symbols of each slot, $T_{\text{data}} = \frac{1}{\Delta f}$ denotes the symbol duration, and T_{cp} represents the length of CP. Then, the signal is transmitted from the BS to the vehicle. The received signal is given by

$$\mathbf{y} = \sqrt{\gamma}\,\mathbf{H_s}\mathbf{x} + \mathbf{z} \tag{2}$$

where $\gamma = \frac{P_t H_L}{\sigma_z^2}$ denotes the signal-to-noise ratio (SNR), P_t means the transmit power, σ_z^2 is the noise power, H_L represents the large-scale fading parameter [12], $\mathbf{H_s} = [H_{qp}(t,f)]_{N_r \times N_t}$ is the matrix of time-varying channel transfer functions (CTFs), $H_{qp}(t,f)$ is the normalized CTF at instant t from the p-th ($p = 1, 2, ..., N_t$) antenna (A_p^T) at Tx to the q-th ($q = 1, 2, ..., N_r$) antenna (A_q^R) at Rx, $\mathbf{x}$, $\mathbf{y}$, and $\mathbf{z}$ are vectors of the transmitted signal, received signal, and AWGN following $\mathcal{CN}(0,1)$, respectively. In addition, the maximum likelihood detector are utilized to detect $\mathbf{x}$ based on $\mathbf{y}$ [10].

B. Channel Estimation Error Model and 6GPCM

As shown in Fig. 1, the entire communication period is composed of the channel estimation period T_e and data transmission period T_s. During the channel estimation period, pilot symbols are transmitted from the BS to the vehicle to obtain the CSI. We assume that the vehicle can obtain the same CSI once channel estimation is finished. The acquired CSI can be utilized in the following data transmission period. Meanwhile, the BS obtains environmental characteristics through multiple sensors during the channel estimation period, especially velocities of the vehicle user. According to the above assumptions, the BS and vehicle will obtain the estimated CTF $\hat{H}_{qp}(T_e, f)$ at instant T_e and frequency f. We assume that the BS can acquire CSI without errors at instant T_e, i.e., $\hat{H}_{qp}(T_e, f) = H_{qp}(T_e, f)$. Due to the mobility of the vehicle user, the actual CTF $H_{qp}(t, f)$ is time-varying. Therefore, $H_{qp}(t, f)$ is different from the $\hat{H}_{qp}(T_e, f)$ during transmission period T_s, i.e., $H_{qp}(t, f) \neq \hat{H}_{qp}(T_e, f),\ T_e < t \leq T_e + T_s$. According to the channel estimation error model, the actual CTF can be expressed as [9]

$$\begin{aligned} H_{qp}(t,f) =& \hat{H}_{qp}(T_e,f)|R_{qp}(T_e,\Delta t)| \\ &+ H_{\text{i},qp}\sqrt{1-|R_{qp}(T_e,\Delta t)|^2} \end{aligned} \tag{3}$$

where $|\cdot|$ calculates the absolute value, $\Delta t = t - T_e,\ T_e \leq t \leq T_e + T_s$ is the time difference, $H_{\text{i},qp} \sim \mathcal{CN}(0,1)$ represents the independent innovation component, and the estimated 6GPCM CTF can be given by [12]

$$\begin{aligned} \hat{H}_{qp}(T_e,f) =& \sqrt{\frac{K(T_e)}{K(T_e)+1}} H_{qp}^{\text{LoS}}(T_e,f) \\ &+ \sqrt{\frac{1}{K(T_e)+1}} H_{qp}^{\text{NLoS}}(T_e,f) \end{aligned} \tag{4}$$

where $K(t)$ is the K-factor at instants t, $H_{qp}^{\text{LoS}}(t,f)$ and $H_{qp}^{\text{NLoS}}(t,f)$ are line-of-sight (LoS) and non-LoS (NLoS) components, respectively. Furthermore, the channel time ACF $R_{qp}(T_e, \Delta t)$ of the 6GPCM can be expressed as [13]

$$\begin{aligned} R_{qp}(t,\Delta t) &\triangleq \mathbb{E}\{H_{qp}(t,f)H_{qp}^*(t+\Delta t,f)\} \\ &= \sqrt{\frac{K(t)}{K(t)+1}\cdot\frac{K(t+\Delta t)}{K(t+\Delta t)+1}} R_{qp}^{\text{LoS}}(t,\Delta t) \\ &+ \sqrt{\frac{1}{K(t)+1}\cdot\frac{1}{K(t+\Delta t)+1}} R_{qp}^{\text{NLoS}}(t,\Delta t) \end{aligned} \tag{5}$$

where the operator $\mathbb{E}\{\cdot\}$ calculates the expectation value, $R_{qp}^{\text{LoS}}(t,\Delta t)$ and $R_{qp}^{\text{NLoS}}(t,\Delta t)$ are given by [13]

$$R_{qp}^{\text{LoS}}(t,\Delta t) = e^{j2\pi\frac{(f_c-f)[D_{qp}(t)-D_{qp}(t+\Delta t)]}{\lambda f_c}} \tag{6}$$

$$\begin{aligned} R_{qp}^{\text{NLoS}}(t,\Delta t) = P_{\text{surv}}(\Delta t)\cdot\mathbb{E}\Bigg[\sum_{n=1}^{N_{qp}(t)}\sum_{m=1}^{M_n(t)}\sqrt{P_{qp,m_n}(t)} \\ \sqrt{P_{qp,m_n}(t+\Delta t)}e^{j2\pi\frac{(f_c-f)[d_{qp,m_n}(t)-d_{qp,m_n}(t+\Delta t)]}{\lambda f_c}}\Bigg] \end{aligned} \tag{7}$$

where f_c denotes the carrier frequency, λ means the signal wavelength, $P_{\text{surv}}(\Delta t)$ is the survival probability of clusters,

$N_{qp}(t)$ represents the number of clusters between A_p^T and A_q^R, $M_n(t)$ is the number of rays in the n-th cluster, $P_{qp,m_n}(t)$ is the power of the m-th ray in the n-th path, $D_{qp}(t)$ is distance between A_p^T and A_q^R, and $d_{qp,m_n}(t)$ is distance from A_p^T, passing through cluster pairs, to A_q^R.

According to the channel estimation error model, the matrix of time-varying CTFs $\mathbf{H_s}$ can be represented as

$$\mathbf{H_s} = \mathbf{H_e} \odot \mathbf{R} + \mathbf{H_i} \odot \mathbf{R_i} \tag{8}$$

where $\odot$ means Hadamard product. Here, $\mathbf{H_e}$, $\mathbf{H_i}$, $\mathbf{R}$, and $\mathbf{R_i}$ are given by

$$\begin{cases} \mathbf{H_e} = & \left[\hat{H}_{qp}(T_e, f)\right]_{N_r \times N_t} \\ \mathbf{R} = & \left[|R_{qp}(T_e, \Delta t)|\right]_{N_r \times N_t} \\ \mathbf{H_i} = & \left[H_{\mathrm{i},qp}\right]_{N_r \times N_t} \\ \mathbf{R_i} = & \left[\sqrt{1 - |R_{qp}(T_e, \Delta t)|^2}\right]_{N_r \times N_t} \end{cases}. \tag{9}$$

This model ensures the continuity of channel temporal variation and can characterize the channel temporal variation based on the time ACF of 6GPCM, simultaneously. By substituting (8) into (2), we can obtain

$$\mathbf{y} = \sqrt{\gamma}\left[\mathbf{H_e} \odot \mathbf{R} + \mathbf{H_i} \odot \mathbf{R_i}\right]\mathbf{x} + \mathbf{z}. \tag{10}$$

III. Performance Metrics of URLLC Systems

In this section, based on the receive signal (10), we will derive the expression of ABEP of uRLLC systems over time-varying channels. Then, transmission blocklength designs under reliability constraints are shown according to the expression of ABEP. Furthermore, the ADR and transmission latency are given.

A. ABEP

The ABEP is considered as the indicator of the reliability. In this subsection, the expression of ABEP is derived and the impacts of SNR, channel time ACF and mobility on ABEP are analyzed. Without loss of generality, the ABEP can be analytically expressed as [3]

$$\mathrm{ABEP} \approx \sum_{m=1}^{M}\sum_{\hat{m}=1}^{M} \frac{\mathcal{N}_{(m\to\hat{m})}\mathrm{PEP}_{(m\to\hat{m})}}{M\log_2(M)} \tag{11}$$

where M is the modulation order, $\mathcal{N}_{(m\to\hat{m})}$ denotes the Hamming distance between the modulation symbol s_m and demodulation symbol $s_{\hat{m}}$ detected by the detector.

The $\mathrm{PEP}_{(m\to\hat{m})}$ over single-input multiple-output (SIMO) channels is given by [10], [15]

$$\begin{aligned}\mathrm{PEP}_{(m\to\hat{m})} &\triangleq ||\mathbf{y} - \sqrt{\gamma}\hat{\mathbf{h}} \odot \mathbf{r}\, s_m||^2 > ||\mathbf{y} - \sqrt{\gamma}\hat{\mathbf{h}} \odot \mathbf{r}\, s_{\hat{m}}||^2 \\ &= \mathrm{Q}\left(\sqrt{\frac{||\sqrt{\gamma}\hat{\mathbf{h}} \odot \mathbf{r}||^2 |s_m - s_{\hat{m}}|^2}{2\gamma\left(1 - ||\mathbf{r}||^2\right)|s_m|^2 + 2}}\right)\end{aligned} \tag{12}$$

where $||\cdot||$ calculates the Frobenius norm, $\hat{\mathbf{h}}$ and $\mathbf{r}$ are vectors of estimated CTF and channel time ACF, respectively. Here, $\mathrm{Q}(\cdot) = \int_x^{+\infty} \frac{1}{\sqrt{2\pi}} e^{-\frac{t^2}{2}}\,\mathrm{d}t$ is Q function.

Furthermore, according to system model (10) and the PEP (12), the PEP over MIMO channels can be expressed as

$$\mathrm{PEP}_{(m\to\hat{m})} = \mathrm{Q}\left(\sqrt{\frac{||\sqrt{\gamma}\mathbf{H_e} \odot \mathbf{R}||^2 |s_m - s_{\hat{m}}|^2}{2\gamma\left(||\mathbf{R_i} \odot \mathbf{R_i}||\right)|s_m|^2 + 2}}\right). \tag{13}$$

In this paper, the MPSK modulation with $|s_m|^2 = 1$ and $|s_m - s_{\hat{m}}|^2 = 2 - 2\cos\frac{m-\hat{m}}{M}$ is considered. Substituting them into (13), we can obtain

$$\mathrm{PEP}_{(m\to\hat{m})} = \mathrm{Q}\left(\sqrt{\frac{||\mathbf{H_e} \odot \mathbf{R}||^2\left(1 - \cos\frac{\hat{m}-m}{M}\right)}{\left(||\mathbf{R_i} \odot \mathbf{R_i}||\right) + 1/\gamma}}\right). \tag{14}$$

1) SNR: Note that the PEP approaches the bound with the increasing SNR γ. The bound can be expressed as

$$\lim_{\gamma\to+\infty}\mathrm{PEP}_{(m\to\hat{m})} = \mathrm{Q}\left(\sqrt{\frac{||\mathbf{H_e} \odot \mathbf{R}||^2\left(1 - \cos\frac{\hat{m}-m}{M}\right)}{\left(||\mathbf{R_i} \odot \mathbf{R_i}||\right)}}\right). \tag{15}$$

Therefore, the ABEP also has the bound with the increasing SNR according to (11). This phenomenon reveals that it is crucial to adopt a comprehensive strategy to improve the PEP instead of merely concentrating on the improvement of SNR. The mobility, modulation orders, and transmission periods need to be considered to enhance the PEP.

2) Channel Time ACF: According to (14), the channel time ACF is a direct factor affecting the PEP. Obviously, the first-order derivative demonstrates that the PEP monotonically increases with the growing channel time ACF. In addition, there is an extreme situation. When $\mathbf{R}$ approaches $\mathbf{A_1} = [1]_{N_r \times N_t}$, $\mathbf{R_i}$ will tend towards zero matrix. Therefore, we can obtain

$$\lim_{\mathbf{R}\to\mathbf{A_1}}\mathrm{PEP}_{(m\to\hat{m})} = \mathrm{Q}\left(\sqrt{\gamma||\mathbf{H_e}||^2\left(1 - \cos\frac{\hat{m}-m}{M}\right)}\right). \tag{16}$$

Under this condition, the channel estimation is perfect and channel CTFs remain constant during the transmission period, which is consistent with the quasi-static channel assumption during one block in the literature. The performance analysis considering the time-varying channel time ACF in this paper is more generalized.

3) Mobility: The channel time ACF reduces with the increasing mobility [13]. Furthermore, we derive the expression of the PEP of uRLLC systems utilizing the MPSK modulation in mobility scenarios.

Distance differences in (5) can be approximated as

$$D_{qp,m_n}(t) - D_{qp,m_n}(t+\Delta t) \approx ||\vec{v}^{\mathrm{Tx}} + \vec{v}^{\mathrm{Rx}}||\,\Delta t\,\psi_{qp,(\mathrm{Tx}\to\mathrm{Rx})} \tag{17}$$

$$\begin{aligned} &d_{qp,m_n}(t) - d_{qp,m_n}(t+\Delta t) \\ &\quad\approx ||\vec{v}^{\mathrm{Tx}} + \vec{v}^{A_n} + \vec{v}^{C_n} + \vec{v}^{\mathrm{Rx}}||\,\Delta t\,\psi_{qp,(\mathrm{Tx}\to A_n\to Z_n\to\mathrm{Rx})}\end{aligned} \tag{18}$$

where $\vec{v}^{\mathrm{Tx}}$, $\vec{v}^{A_n}$, $\vec{v}^{Z_n}$, and $\vec{v}^{\mathrm{Rx}}$ are velocity vectors of the Tx, first-bounce cluster A_n, last-bounce cluster Z_n, and Rx, respectively. Also, $\psi_{qp,(\mathrm{Tx}\to\mathrm{Rx})}$ and $\psi_{qp,(\mathrm{Tx}\to A_n\to Z_n\to\mathrm{Rx})}$ are trajectory factors.

$$\mathrm{PEP}=\mathrm{Q}\left\{\sqrt{\frac{\sum_{q=1}^{N_r}\sum_{p=1}^{N_t}\left|\hat{H}_{qp}(T_e,f)\left\{F_{\mathrm{LoS}}e^{j2\pi Av_1\Delta t}+F_{\mathrm{NLoS}}e^{-\lambda_R\left(\frac{v_1\Delta t}{D_c^S}+B\right)}\mathbb{E}\left[\sum_{n=1}^{N_{qp}(t)}\sum_{m=1}^{M_n(t)}Ee^{(C+j2\pi A)v_2\Delta t+D}\right]\right\}\right|^2\left(1-\cos\frac{\hat{m}-m}{M}\right)}{\sqrt{\sum_{q=1}^{N_r}\sum_{p=1}^{N_t}\left|1-\left\{F_{\mathrm{LoS}}e^{j2\pi Av_1\Delta t}+F_{\mathrm{NLoS}}e^{-\lambda_R\left(\frac{v_1\Delta t}{D_c^S}+B\right)}\mathbb{E}\left[\sum_{n=1}^{N_{qp}(t)}\sum_{m=1}^{M_n(t)}Ee^{(C+j2\pi A)v_2\Delta t+D}\right]\right\}\right|^2}+1/\gamma}\right\} \tag{24}$$

The antenna element spacing equals to half wavelength in this paper. Therefore, the survival probability of clusters also can be approximated as

$$P_{\mathrm{surv}}(\Delta t)\approx e^{-\lambda_R\left[\Delta t\left(\frac{||\vec{v}^{\mathrm{Tx}}+\vec{v}^{\mathrm{Rx}}||}{D_c^S}\right)+\lambda\frac{(p-1)\cos\beta_E^T+(q-1)\cos\beta_E^R}{2D_c^A}\right]} \tag{19}$$

where, λ_R is the recombination rate of clusters, D_c^S and D_c^A are coefficients describing the channel spatial correlation, β_E^T and β_E^R are elevation angles of the antenna array at Tx and Rx, respectively.

Furthermore, (5) can be expressed as

$$R_{qp}(t,\Delta t)=\underbrace{F_{\mathrm{LoS}}\ e^{j2\pi Av_1\Delta t}}_{\text{LoS term}}+\underbrace{F_{\mathrm{NLoS}}\ e^{-\lambda_R\left[\frac{v_1\Delta t}{D_c^S}+B\right]}\mathbb{E}\left[\sum_{n=1}^{N_{qp}(t)}\sum_{m=1}^{M_n(t)}Ee^{(C+j2\pi A)v_2\Delta t+D}\right]}_{\text{NLoS term}} \tag{20}$$

where specific expressions of v_1, v_2, F_{LoS}, F_{NLoS}, A, B, C, D, and E are given by (21)–(23).

$$\begin{cases}v_1 = & ||\vec{v}^{\mathrm{Tx}}+\vec{v}^{\mathrm{Rx}}||\,\psi_{qp,(\mathrm{Tx}\to\mathrm{Rx})}\\ v_2 = & ||\vec{v}^{\mathrm{Tx}}+\vec{v}^{A_n}+\vec{v}^{C_n}+\vec{v}^{\mathrm{Rx}}||\,\psi_{qp,(\mathrm{Tx}\to A_n\to Z_n\to\mathrm{Rx})}\end{cases} \tag{21}$$

$$\begin{cases}F_{\mathrm{LoS}} = & \sqrt{\frac{K(t)}{K(t)+1}\cdot\frac{K(t+\Delta t)}{K(t+\Delta t)+1}}\\ F_{\mathrm{NLoS}} = & \sqrt{\frac{1}{K(t)+1}\cdot\frac{1}{K(t+\Delta t)+1}}\end{cases} \tag{22}$$

$$\begin{cases}A = & \frac{f_c-f}{\lambda f_c}\\ B = & \frac{\lambda[(p-1)\cos(\beta_E^T)+(q-1)\cos(\beta_E^R)]}{2D_c^A}\\ C = & -\frac{r_\tau-1}{2c\,r_\tau\mathrm{DS}}\\ D = & -\frac{Z_n}{10}\ln 10\\ E = & \sqrt{P_{qp,m_n}(t)P_{qp,m_n}(t+\Delta t)}\end{cases} \tag{23}$$

where DS denotes the delay spread, r_τ is the delay distribution proportionality, and Z_n means the cluster shadowing [12].

Furthermore, by substituting (20)–(23) into (14), we can obtain the expression of PEP considering velocities v_1 and v_2 as shown in (24). Note that A, B, C, D, E, F_{LoS}, and F_{NLoS} are independent of velocities v_1 and v_2 according to (22) and (23). The increasing v_1 or v_2 will result in the exponential decline of the NLoS term. However, the absolute value of the LoS term keep unchanged whatever velocities are. Moreover, the expression of the ABEP can be obtained by substituting (24) into (11).

B. Maximal Data Transmission Period

Based on the expression of the ABEP, we can flexibly design different transmission blocklengths under different reliability constraints. The channel time ACF decreases with increasing time difference Δt. Therefore, the ABEP degrades with increasing time difference Δt. In order to satisfy the quality of communication service, the maximal data transmission period can be given by

$$T_s=\max\left\{\Delta t\,\middle|\,\mathrm{ABEP}(\Delta t)=\epsilon_{\mathrm{th}}\right\} \tag{25}$$

where ϵ_{th} is the error threshold. Then according to the (1), we can obtain the transmission blocklength.

C. Average ADR

The data rate is considered as the fundamental performance metric to characterize the effectiveness of communication systems. In short block regime, the instantaneous ADR can be expressed as [6]

$$R(t)\approx C(t)-\sqrt{\frac{\gamma\,(2+\gamma)}{(1+\gamma)^2N_b}}\,Q^{-1}(\mathrm{ABEP})+\frac{\log_2 N_b}{2N_b} \tag{26}$$

where $C(t)=\log_2\left\{\det(\mathbf{I}+\gamma\mathbf{H_s}\mathbf{H_s}^H)\right\}$ is the instantaneous channel capacity, $\mathbf{I}$ is the identity matrix.

Due to the time-varying characteristic of instantaneous ADR, it is inconvenient to describe the effectiveness through instantaneous ADR. Therefore, the ratio $\tilde{R}/\tilde{C}$ is seen as an indicator to characterize the effectiveness of uRLLC systems, where the average channel capacity $\tilde{C}=\int_0^{T_e+T_s}C(t)\,\mathrm{d}t/\left(T_e+T_s\right)$ and the average ADR can be calculated by

$$\begin{aligned}\tilde{R}\triangleq&\frac{\int_{T_e}^{T_e+T_s}R(t)\,\mathrm{d}t}{T_e+T_s}\\ \approx&\frac{\sum_j^{n_{\mathrm{slot}}}\sum_{i_j}^{n_{\mathrm{sym}}}\int_{i_j(T_{\mathrm{data}}+T_{\mathrm{cp}})+(j-1)T_{\mathrm{slot}}-T_{\mathrm{data}}}^{i_j(T_{\mathrm{data}}+T_{\mathrm{cp}})+(j-1)T_{\mathrm{slot}}}C(t)\,dt}{T_e+T_s}\\ &+\frac{T_s\,T_{\mathrm{data}}\left(\sqrt{\frac{\gamma\,(2+\gamma)}{(1+\gamma)^2N_b}}\,Q^{-1}(\epsilon_{\mathrm{th}})+\frac{\log_2 N_b}{2N_b}\right)}{\left(T_e+T_s\right)\left(T_{\mathrm{cp}}+T_{\mathrm{data}}\right)}.\end{aligned} \tag{27}$$

D. Transmission Latency

The transmission latency is the fundamental performance indicator of uRLLC systems, which is defined as the duration required for transmitting D bits data and can be given by [5]

$$t_{\mathrm{latency}}=\frac{D}{\tilde{R}} \tag{28}$$

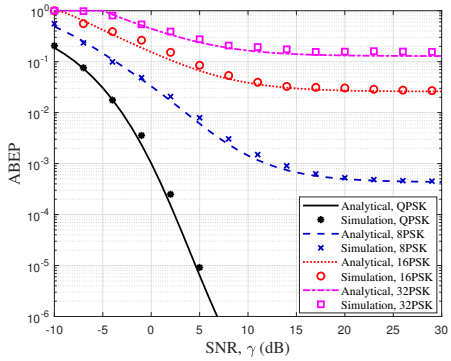

Fig. 2. ABEP with different modulation orders w.r.t. SNR ($v^{\mathrm{Rx}} = 10$ m/s, $\Delta t = 1$ ms, $N_{\mathrm{sim}} = 10^6$).

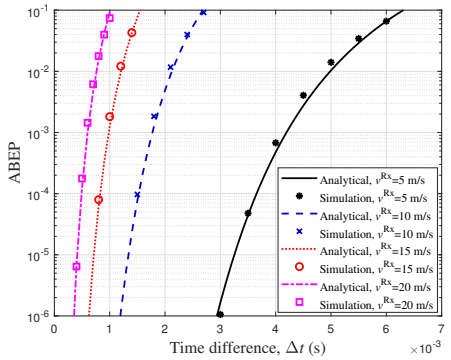

Fig. 3. ABEP with different speeds of Rxs w.r.t. time difference ($M = 4$, SNR = 10 dB, $N_{\mathrm{sim}} = 10^6$).

IV. Results and Analysis

This section shows results and analysis for performance metrics of uRLLC systems discussed above i.e., the ABEP and ratios of average ADR to average capacity. The expression (24) is validated by Monte Carlo simulations according to the definition in (12). The number of Monte Carlo simulations N_{sim} is set as 10^6. The parameter settings of the channel environment, antenna array, and system configuration are based on [13] and [16]. Specific parameters are as follows: carrier frequency $f_c = 5.3$ GHz, antenna spacing of Tx/Rx $\delta_T, \delta_R = 0.0283$ m, numbers of Tx/Rx $N_t, N_r = 2$, azimuth/elevation angles of Tx/Rx antenna array $\beta_A^T, \beta_A^R, \beta_E^T, \beta_E^R = \pi/4$, the initial number of clusters $N_{qp}(t_0) = 10$, the subcarrier spacing $\Delta f = 60$ kHz, the number of subcarriers $n_f = 512$, the direction vector of motion for Rx $\vec{v}^{\mathrm{Rx}}/||\vec{v}^{\mathrm{Rx}}||$ = (1, 0, 0). Also, initial positions of Tx and Rx are (0, 0, 20) m and (-10, -10, 1) m, respectively.

Fig. 2 shows comparisons between the ABEP of uRLLC systems utilizing different modulation orders, i.e., QPSK, 8PSK, 16PSK, and 32PSK. With SNR increasing from 15 dB to 30 dB, there are marginal performance enhancements of the ABEP of uRLLC systems utilizing 8PSK, 16PSK, and 32PSK, which indicates obvious bounds of the ABEP of uRLLC systems with the increasing SNR.

Fig. 3 illustrates the ABEP with different speeds of Rxs w.r.t. time difference. As shown in Fig. 3, there is sharp degradation of the ABEP with increasing time difference within several milliseconds. This phenomenon results from the channel time ACF decreases fast within several milliseconds.

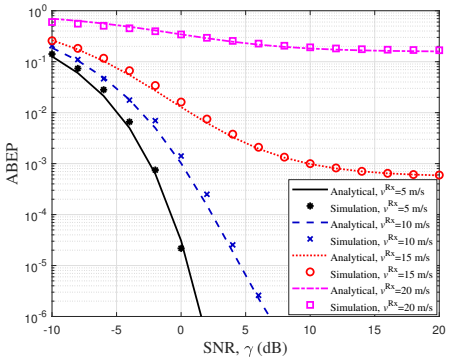

Fig. 4. ABEP with different speeds of Rxs w.r.t. SNR ($M = 4$, Δt = 1 ms, $N_{\mathrm{sim}} = 10^6$).

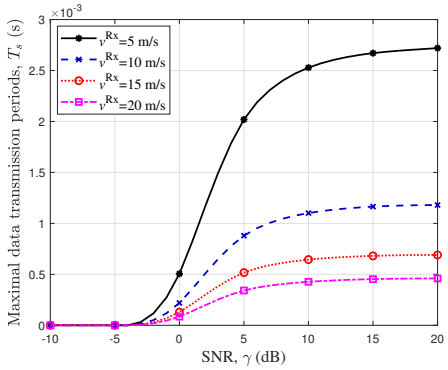

Fig. 5. Maximal transmission periods with different speeds of Rx ($M = 4$, $\epsilon_{\mathrm{th}} = 10^{-5}$).

The ABEP with different speeds of Rxs w.r.t SNR is shown in Fig. 4. The ABEP increases from 2.17×10^{-5} to 3.42×10^{-1} when v^{Rx} grows from 5 m/s to 20 m/s with SNR = 0 dB, which represents considerable discrepancies between the ABEP with different speeds of Rx. In addition, there are bounds of the ABEP with the increasing SNR when $v^{\mathrm{Rx}} = 20$ m/s and $v^{\mathrm{Rx}} = 15$ m/s, which is consistent with the above analysis. Note that bounds of the ABEP cannot be observed when $v^{\mathrm{Rx}} = 10$ m/s and $v^{\mathrm{Rx}} = 5$ m/s for the reason that their bounds may be less than 10^{-6}. Simulation results in Fig. 2 and Fig. 4 have validated the analysis of (15).

Fig. 5 shows maximal transmission periods with different v^{Rx} under the reliability constraint ϵ_{th}. Enhancements of maximal transmission periods are slight when SNR exceeds 10 dB. Moreover, maximal transmission periods equal to zero when SNR ≤ -5 dB due to the constraint of reliability. This indicates that there are no transmission periods satisfying the reliability constraint (25) when SNR ≤ -5 dB. There are huge gaps between maximal transmission periods with $v^{\mathrm{Rx}} = 5$ m/s and others. However, disparities among $v^{\mathrm{Rx}} = 10$ m/s, $v^{\mathrm{Rx}} = 15$ m/s, and $v^{\mathrm{Rx}} = 20$ m/s are inconspicuous.

Ratios of average ADR to average capacity with different v^{Rx} are compared in Fig. 6. Transmission periods with different v^{Rx} can be obtained as depicted in Fig. 5. System parameters, including T_{cp}, Δf, n_f, and n_{sym}, are set according

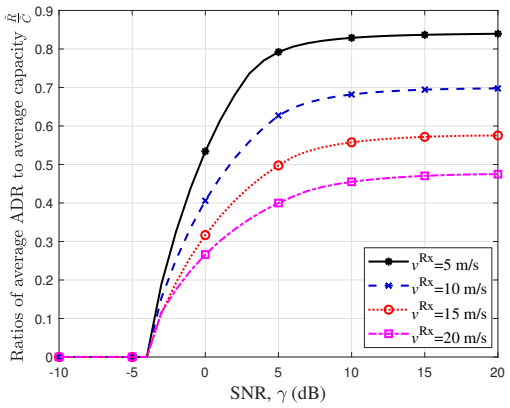

Fig. 6. Average ADRs with different speeds of Rx ($M = 4$, $\epsilon_{\mathrm{th}} = 10^{-5}$, $T_{\mathrm{e}} = 0.5$ ms, $T_{\mathrm{cp}} = 1.1905$ us, $\Delta f = 60$ kHz, $n_f = 512$, $n_{\mathrm{sym}} = 14$).

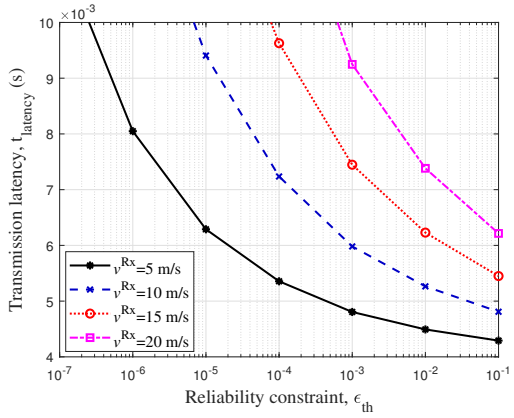

Fig. 7. Latency with different speeds of Rx w.r.t. reliability constraints ($M = 4$, $T_{\mathrm{e}} = 0.5$ ms, $T_{\mathrm{cp}} = 1.1905$ us, $\Delta f = 60$ kHz, $n_f = 512$, $n_{\mathrm{sym}} = 14$, $D = 1$ Mbit).

to [16]. We observe that, with SNR $= 10$ dB, ratios decrease from 82.7% to 45.2% when v^{Rx} increases from 5 m/s to 20 m/s. Moreover, there are merely slight enhancements of ratios with the increasing SNR within a high SNR regime.

Fig. 7 illustrates the tradeoff between the transmission latency and reliability constraint. Note that there are lower bounds of the transmission latency. In addition, with the decreasing error probability, discrepancies of transmission latency with different user speeds become larger. This phenomenon indicates that uRLLC in high mobility scenarios is difficult to realize.

V. Conclusions

In this paper, the expression of PEP of uRLLC systems utilizing the MPSK modulation has been derived based on time ACF of the 6GPCM in mobility scenarios. The expression has been validated by Monte Carlo simulations. In addition, we have proposed a new framework for calculation of the average ADR considering the channel estimation period and CP length. Results have shown that the high user mobility results in the degradation of uRLLC system performance metrics. Impacts of user mobility on the ABEP have been surpassed its influences on average ADRs. In addition, bounds of the ABEP with the increasing SNR can be observed. Moreover, enhancements of average ADRs have been marginal with the increasing SNR within a high SNR regime.

Acknowledgment

This work was supported by the National Key R&D Program of China under Grant 2021YFB2900300, the National Natural Science Foundation of China (NSFC) under Grants 61960206006, and 62271147, the Fundamental Research Funds for the Central Universities under Grant 2242022k60006 and 2242023K5003, the Key Technologies R&D Program of Jiangsu (Prospective and Key Technologies for Industry) under Grants BE2022067 and BE2022067-1, the Start-up Research Fund of Southeast University under Grant RF1028623029, and the Research Fund of National Mobile Communications Research Laboratory, Southeast University, under Grant 2024A05.

References

[1] ITU-R, IMT Vision – The ITU-R Framework for IMT-2030, July 2023. [Online]. Available: https://www.itu.int/en/ITU-R/study-groups/rsg5/rwp5d/imt-2030/Documents/IMT-2030.

[2] C.-X. Wang, *et al.*, "On the road to 6G: Visions, requirements, key technologies and testbeds," *IEEE Commun. Surveys Tuts.*, vol. 25, no. 2, pp. 905–974, 2nd Quart. 2023.

[3] J. Zhang, *et al.*, "Generalized polarization-space modulation," *IEEE Trans. Commun.*, vol. 68, no. 1, pp. 258–273, Jan. 2020.

[4] H. Ji, S. Park, J. Yeo, Y. Kim, J. Lee, and B. Shim, "Ultra-reliable and low-latency communications in 5G downlink: Physical layer aspects," *IEEE Wireless Commun.*, vol. 25, no. 3, pp. 124–130, June 2018.

[5] G. Durisi, T. Koch, and P. Popovski, "Toward massive, ultrareliable, and low-latency wireless communication with short packets," *Proc. IEEE*, vol. 104, no. 9, pp. 1711–1726, Sept. 2016.

[6] Y. Polyanskiy, H. V. Poor, and S. Verdu, "Channel coding rate in the finite blocklength regime," *IEEE Trans. Inf. Theory*, vol. 56, no. 5, pp. 2307–2359, May 2010.

[7] A. Collins and Y. Polyanskiy, "Coherent multiple-antenna block-fading channels at finite blocklength," *IEEE Trans. Inf. Theory*, vol. 65, no. 1, pp. 380–405, Jan. 2019.

[8] T. Wu, X. Fan, J. Zeng, W. Ni, and R. P. Liu, "Enabling uRLLC under $\kappa - \mu$ shadowed fading," in *Proc. ICT'28*, London, United Kingdom, June 2021, pp. 1–6.

[9] A. Goldsmith, *Wireless Communications*. Cambridge: Cambridge University Press, 2005.

[10] S. Yang, Z. Zhang, J. Zhang, X. Chu, and J. Zhang, "Adaptive modulation for wobbling UAV air-to-ground links in millimeter-wave bands," *IEEE Internet Things J.* early access, 2024.

[11] C.-X. Wang, J. Huang, H. Wang, X.-Q. Gao, X.-H. You, and Y. Hao, "6G wireless channel measurements and models: Trends and challenges," *IEEE Veh. Technol. Mag.*, vol. 15, no. 4, pp. 22–32, Dec. 2020.

[12] C.-X. Wang, Z. Lv, X.-Q. Gao, X.-H. You, Y. Hao, and H. Haas, "Pervasive wireless channel modeling theory and applications to 6G GBSMs for all frequency bands and all scenarios," *IEEE Trans. Veh. Technol.*, vol. 71, no. 9, pp. 9159–9173, Sept. 2022.

[13] C.-X. Wang, Z. Lv, Y. Chen, and H. Haas, "A complete study of space-time-frequency statistical properties of the 6G pervasive channel model," *IEEE Trans. Commun.*, vol. 71, no. 12, pp. 7273–7287, Dec. 2023.

[14] Y. Fu, *et al.*, "BER performance of spatial modulation systems under 3-D V2V MIMO channel models," *IEEE Trans. Veh. Technol.*, vol. 65, no. 7, pp. 5725–5730, July 2016.

[15] S. Yang, Z. Zhang, J. Zhang, and J. Zhang, "Impact of rotary-wing UAV wobbling on millimeter-wave air-to-ground wireless channel," *IEEE Trans. Veh. Technol.*, vol. 71, no. 9, pp. 9174–9185, Sept. 2022.

[16] *Physical channels and modulation (Release 18)*, document TS 38.211, V18.1.0, 3GPP, Dec. 2023.